Multidisciplinary Journal of Engineering and Technology
ISSN: 3007-6900
DOI: https://doi.org/10.61784/mjet3021

THERMAL EFFECTS ON THE LD END-FACE PUMPED ND:YAG LASER MEDIUM

XingYu Liu*, JianSheng Zhang, Wen Du
School of Basic Science, Xi 'an Technological University, Xi 'an 710021, Shaanxi, China.
Corresponding Author: XingYu Liu, Email: a2210211003@163.com

Abstract: Solid-state lasers are widely used in various industries due to their high stability, compact structure, and excellent beam quality. However, thermal effects have long been a significant constraint on improving laser performance. Thermal effects are primarily caused by the heat deposition resulting from the absorption of pump energy by the laser medium in solid-state lasers. Studying the heat conduction equation of the laser medium is crucial for understanding thermal effects. This paper provides a detailed theoretical derivation for calculating the heat conduction equation of the laser medium in solid-state lasers. A series expansion is used to derive the analytical expression for the heat conduction equation, and the fourth-order Runge-Kutta method is employed to numerically solve it. The temperature simulation results of the laser medium end face using both methods are compared to verify the correctness of the analytical derivation process and to analyze the causes of any errors.
Keywords: Heat conduction equation; Power series; Runge-Kutta; Temperature simulation

1 INTRODUCTION

In recent years, solid-state lasers based on Nd:YAG crystals have gained wide applications due to their excellent beam quality, high stability, and compact design. These lasers are commonly used in fields such as material processing, medical treatments, and scientific research. However, one of the key challenges in the performance of these lasers is the thermal effects caused by the pumping process. A series of effects caused by the change in the end-face temperature gradient are referred to as the thermal effects of the laser [1-3]. When the laser diode (LD) pumps the Nd:YAG medium, the energy absorbed from the pump light generates heat, leading to a temperature gradient within the laser medium. This temperature gradient can severely affect the laser's efficiency, beam quality, and overall performance, causing phenomena such as thermal lensing, which distorts the laser beam and reduces output power.
Understanding the thermal effects in Nd:YAG laser media is crucial for optimizing laser design and improving its efficiency. As the heat generated by the absorbed pump light is not evenly distributed, the resulting temperature gradient plays a critical role in determining the laser's performance. This study focuses on the thermal effects at the end face of the laser medium under LD pumping, simulating the temperature distribution within the Nd:YAG crystal. The study provides an in-depth analysis of the temperature distribution at the medium's end face under different pump powers and pump beam radii.

2 HEAT CONDUCTION EQUATION OF THE LASER MEDIUM

The laser working substance is an important component of solid-state lasers. The Nd:YAG crystal is chosen for its high mechanical strength, good thermal conductivity, and low laser threshold, making it the subject of this study.

2.1 Establishing the Heat Conduction Equation

The temperature distribution inside the crystal is related to the heat power density generated by the pump light, the thermal properties of the crystal, the geometry, and external conditions [4-8]. Since the selected crystal has isotropic thermal properties and the cylindrical rod has axial symmetry, the steady-state equation and heat source equation in cylindrical coordinates are as follows:

$$\frac{\partial^2 T(r,z)}{\partial r^2}+\frac{1}{r}\frac{\partial T(r,z)}{\partial r}+\frac{\partial^2 T(r,z)}{\partial z^2}=-\frac{q(r,z)}{k} \tag{1}$$

$$\begin{cases} q(r,z)=\alpha\eta I_0 e^{[-2(\frac{r^2}{\omega^2})]} e^{(-\alpha z)} \\ I_0=\dfrac{P}{2\pi\int_0^{\infty} e^{-2\frac{r^2}{\omega^2}} r dr} \end{cases} \tag{2}$$

Where r and z are the radial and axial coordinates of the crystal, respectively, with the origin at the center of the pump face of the crystal, *T(r)* is the temperature, *q(r,z)* is the thermal power density function, PPP represents the pump power, η is the conversion efficiency (value of 0.3), k is the thermal conductivity of the crystal, which is 14 W/(m·K). and α is

the absorption coefficient of the crystal (value of 0.3 cm^{-1}).

The heat variation along the direction of the laser rod's length z ultimately becomes **exp(−αz)**. Given this property, assuming the temperature distribution during the differential process is $T(r,z)=T(r)\cdot T(z)=T(r)exp(-\alpha z)$, we substitute it into equation (1) and obtain:

$$\frac{\partial^2 T(r)e^{-\alpha z}}{\partial r^2}+\frac{1}{r}\frac{\partial T(r)e^{-\alpha z}}{\partial r}+\alpha^2 T(r)e^{-\alpha z}+\frac{\alpha\eta I_0 e^{[-2(\frac{r^2}{\omega^2})]}e^{(-\alpha z)}}{k}=0 \tag{3}$$

Multiply both sides by exp(αz):

$$\frac{d^2T(r)}{dr^2}+\frac{1}{r}\frac{dT(r)}{dr}+\alpha^2 T(r)=-\frac{\alpha\eta I_0 e^{[-2(\frac{r^2}{\omega^2})]}}{k} \tag{4}$$

Set the constant B so that:

$$B=-\frac{\alpha\eta I_0}{k} \tag{5}$$

Now expand the right-hand side of (4) using a Taylor series:

$$\begin{aligned}&-\frac{\alpha\eta I_0}{k}e^{[-2(\frac{r^{2m}}{\omega^{2m}})]}\\ &=B\sum_{n=0}^{\infty}\frac{1}{n!}(-2\frac{r^2}{\omega^2})^n\\ &=\sum_{n=0}^{\infty}B\frac{(-2)^n}{\omega^{2n}*n!}r^{2n}\end{aligned} \tag{6}$$

Assume that $T(r)$ is defined and can be analytically expressed within (r,r_0):

$$\begin{aligned}T(r)&=\sum_{n=0}^{\infty}A_n r^{2n}\\ T'(r)&=\sum_{n=0}^{\infty}(2n)A_n r^{2n-1}\\ T''(r)&=\sum_{n=0}^{\infty}(2n)(2n-1)A_n r^{2n-2}\end{aligned} \tag{7}$$

Substituting (7) into (4), get:

$$\begin{aligned}&\frac{d^2T(r)}{dr^2}+\frac{1}{r}\frac{dT(r)}{dr}+\alpha^2T(r)\\ &=\sum_{n=0}^{\infty}(2n)(2n-1)A_n r^{2n-2}+r^{-1}\sum_{n=0}^{\infty}(2n)A_n r^{2n-1}+\alpha^2\sum_{n=0}^{\infty}A_n r^{2n}\\ &=\sum_{n=0}^{\infty}(2n)(2n-1)A_n r^{2n-2}+\sum_{n=0}^{\infty}(2n)A_n r^{2n-2}+\alpha^2\sum_{n=0}^{\infty}A_n r^{2n}\\ &=\sum_{n=0}^{\infty}(2n)^2A_n r^{2n-2}+\alpha^2\sum_{n=0}^{\infty}A_n r^{2n}\\ &=\sum_{n=0}^{\infty}\left[(2n)^2A_n r^{2n-2}+\alpha^2A_n r^{2n}\right]\end{aligned} \tag{8}$$

From (4), (6), and (8), obtain:

$$\sum_{n=0}^{\infty}\left[(2n)^2A_n r^{2n-2}+\alpha^2A_n r^{2n}\right]=\sum_{n=0}^{\infty}B\frac{(-2)^n}{\omega^{2n}*(n)!}r^{2n} \tag{9}$$

Expanding both sides of (9) to the sixth term:

$$\begin{cases} n=0 & (0^2 A_0 r^{-2} + \alpha^2 A_0 r^0) \\ n=1 & (2^2 A_1 r^0 + \alpha^2 A_1 r^2) \\ n=2 & (4^2 A_2 r^2 + \alpha^2 A_2 r^4) \\ n=3 & (6^2 A_3 r^4 + \alpha^2 A_2 r^6) \\ n=4 & (8^2 A_4 r^6 + \alpha^2 A_2 r^8) \\ n=5 & (10^2 A_5 r^8 + \alpha^2 A_2 r^{10}) \end{cases} \tag{10}$$

Expanding the right-hand side of (9) to the sixth term:

$$\begin{cases} n=0 & B\dfrac{(-2)^0}{\omega^0 * 0!} r^0 \\ n=1 & B\dfrac{(-2)^1}{\omega^2 * 1!} r^2 \\ n=2 & B\dfrac{(-2)^2}{\omega^4 * 2!} r^4 \\ n=3 & B\dfrac{(-2)^3}{\omega^6 * 3!} r^6 \\ n=4 & B\dfrac{(-2)^4}{\omega^8 * 4!} r^8 \\ n=5 & B\dfrac{(-2)^5}{\omega^{10} * 5!} r^{10} \end{cases} \tag{11}$$

By examining equation (9), we find that the power terms of the variables on both sides are integer multiples of 2 starting from zero. Since both sides are equal, we conclude that the coefficients of the same powers of r on both sides are equal:

$$\begin{cases} r^0 & \alpha^2 A_0 + 2^2 A_1 = B\dfrac{(-2)^0}{0!*\omega^0} & A_1 = \left[B\dfrac{(-2)^0}{0!*\omega^0} - \alpha^2 A_0 \right] * \dfrac{1}{4} \\ r^2 & \alpha^2 A_1 + 4^2 A_2 = B\dfrac{(-2)^1}{1!*\omega^2} & A_2 = \left[B\dfrac{(-2)^1}{1!*\omega^2} - \alpha^2 A_1 \right] * \dfrac{1}{16} \\ r^4 & \alpha^2 A_2 + 6^2 A_3 = B\dfrac{(-2)^2}{2!*\omega^4} & A_3 = \left[B\dfrac{(-2)^2}{2!*\omega^4} - \alpha^2 A_2 \right] * \dfrac{1}{36} \\ r^6 & \alpha^2 A_3 + 8^2 A_4 = B\dfrac{(-2)^3}{3!*\omega^6} & A_4 = \left[B\dfrac{(-2)^3}{3!*\omega^6} - \alpha^2 A_3 \right] * \dfrac{1}{64} \\ r^8 & \alpha^2 A_4 + 10^2 A_5 = B\dfrac{(-2)^4}{4!*\omega^8} & A_5 = \left[B\dfrac{(-2)^4}{4!*\omega^8} - \alpha^2 A_4 \right] * \dfrac{1}{100} \end{cases} \tag{12}$$

From equation (12), we obtain A_1 , A_2 , A_3 , A_4 , A_5 , and so on... Let A_0 be the first term of the equation, A_1 be the second term, A_2 be the third term, and so on. By this analogy, we can derive the inverse expression for A_n .

$$A_n = \frac{1}{(2n)^2}\left[B\frac{(-2)^{n-1}}{(n-1)!*\omega^{2n-2}} - \alpha^2 A_{n-1} \right] \tag{13}$$

Simplifying:

$$\begin{cases} T(r) = A_0 + \sum_{n=1}^{\infty} A_n r^{2n} \\ T(r) = A_0 + \sum_{n=1}^{\infty} \left[\dfrac{1}{(2n)^2} \left(B\dfrac{(-2)^{n-1}}{(n-1)!*\omega^{2n-2}} - \alpha^2 A_{(n-1)} \right) \right] r^{2n} \end{cases} \tag{14}$$

Substituting *T(r)* back into *T(r,z)*:

$$\begin{cases} T(r,z) = T(r)\exp(-\alpha z) \\ T(r,\ z) = A_0\exp(-\alpha z) + \exp(-\alpha z)\sum_{n=1}^{\infty}\left[\frac{1}{(2n)^2}\left(B\frac{(-2)^{n-1}}{(n-1)!*\omega^{2n-2}} - \alpha^2 A_{(n-1)}\right)\right]r^{2n} \end{cases} \tag{15}$$

2.2 Boundary Conditions

In this study, the axial variation of the temperature gradient is neglected, and only the radial temperature distribution is considered. Since the heat transfer by convection from the end face to the air is minimal, the effect of convection on the temperature distribution at the end face is ignored. Since the crystal mainly dissipates heat through the side cooling system or cooling water, the side is assumed to be at a constant temperature. The boundary condition is thus determined as:

$$\begin{cases} \left.\frac{dT(r)}{dr}\right|_{r=0} = 0 \\ \left.T(r)\right|_{r=r_0} = T_0 \end{cases} \tag{16}$$

3 LASER MEDIUM END-FACE TEMPERATURE ANALYTICAL SIMULATION

Based on the analytical expression of the laser medium's heat conduction equation derived above, the temperature distribution at the laser medium's end face is simulated, while also exploring the impact of pump power and pump beam radius on the end-face temperature distribution.

3.1 Influence of Pump Power on Medium Temperature Distribution

The variation in pump power significantly affects the heat distribution at the laser medium's end face, leading to thermal lensing effects. Therefore, when using solid-state laser devices to achieve higher output power, it is important to minimize the thermal effects to improve the performance of the laser system. This requires studying the temperature distribution at the end face of the laser medium under different pump powers. Figure 1 shows the three-dimensional temperature distribution of the end face when the radius and length of the Nd:YAG rod are 0.2 cm and 0.5 cm, respectively, with a pump beam radius of 0.5 mm and pump powers of 5W, 10W, 15W, and 20W.

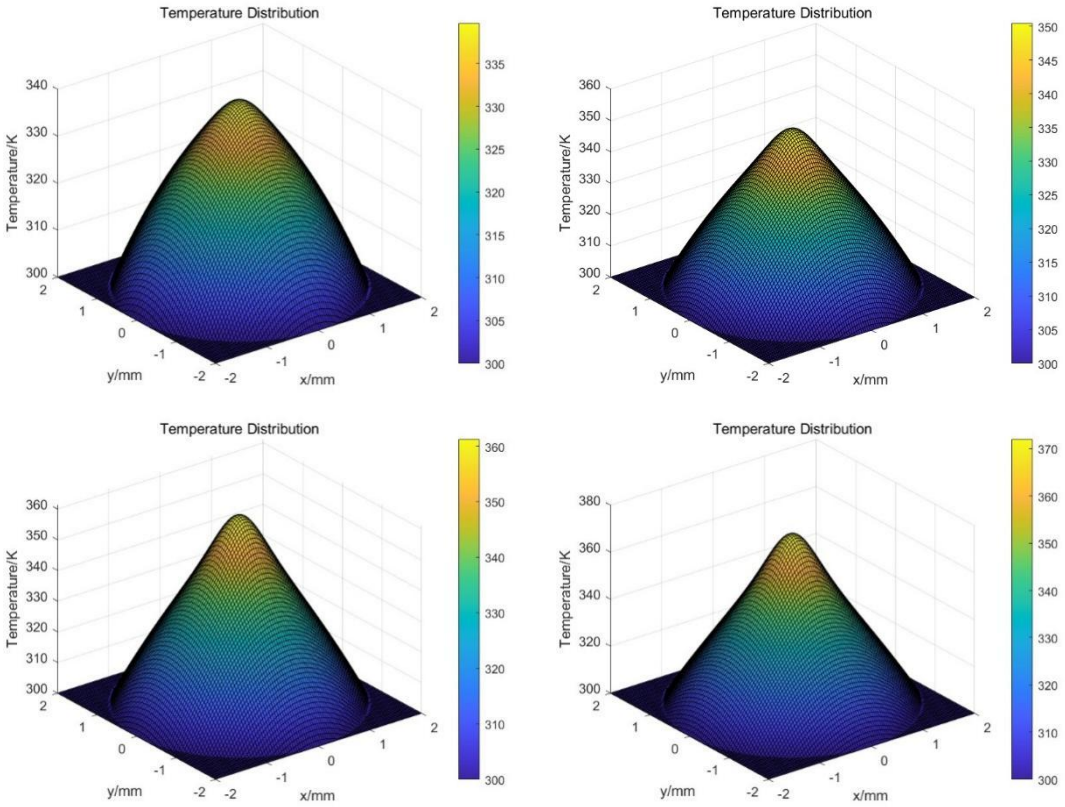

Figure 1 Temperature Distribution at the End-Face of the Laser Medium under Different Pump Powers

From Figure 1, it can be seen that the temperature at the center is the highest, and it increases as the pump power increases. The higher the pump power, the greater the amount of energy absorbed by the laser, leading to more heat accumulation at the smaller end face. The temperature distribution along the radial direction is shown in Figure 2.

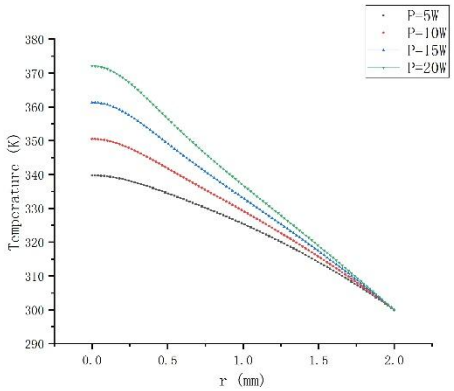

Figure 2 Radial Temperature Distribution of the Laser Medium under Different Pump Powers

Figure 2 shows the heat distribution at the end face of the laser medium under different pump powers. The temperature at the center of the laser medium is 339.73K, 350.52K, 361.32K, and 372.10K for pump powers of 5W, 10W, 15W, and 20W, respectively. As the pump power increases, the temperature at the center of the end face shows an increasing trend. Therefore, in order to ensure the output efficiency and meet the requirements during operation, the pump power should be appropriately reduced.

3.2 Influence of Pump Beam Radius on Medium Temperature Distribution

The change in pump beam radius has a certain impact on the heat source and the quality of the generated laser at the end face. Figure 3 shows the three-dimensional temperature distribution at the end face of the Nd:YAG rod with radii and lengths of 0.2 cm and 0.5 cm, respectively. The pump power is fixed at 10W, and the pump beam radii are 0.05 cm, 0.06 cm, 0.07 cm, and 0.08 cm.

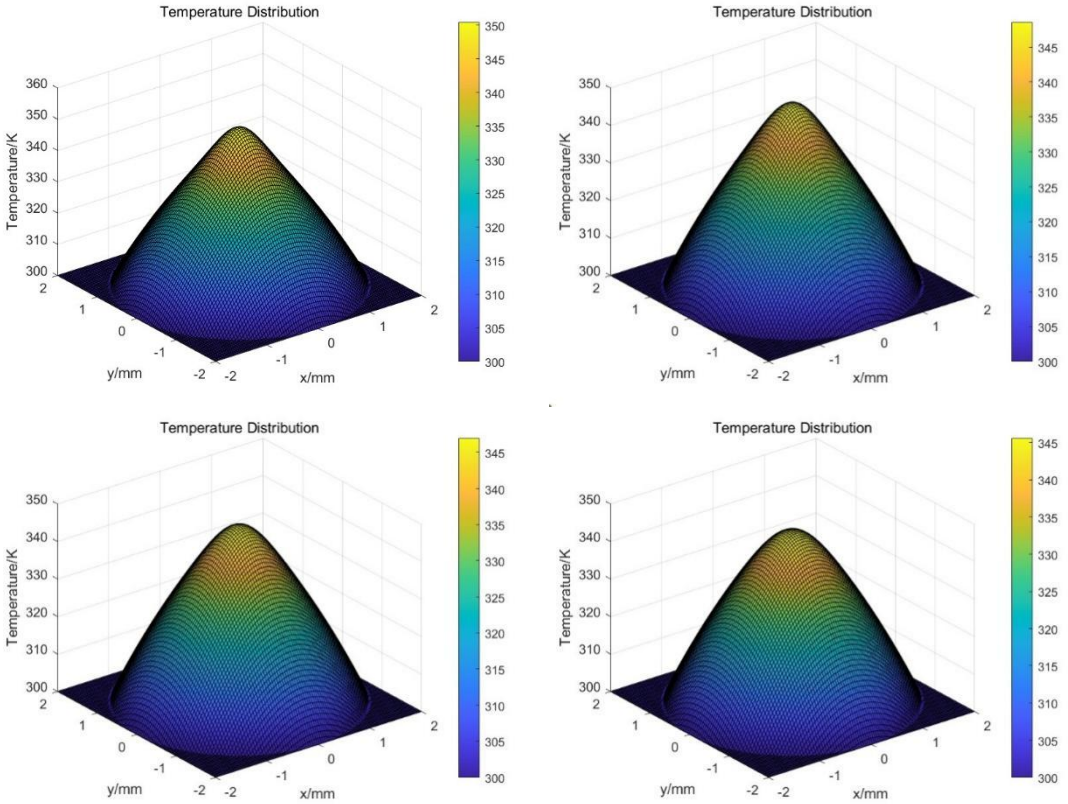

Figure 3 Temperature Distribution at the End-Face of the Laser Medium under Different Pump Beam Radii

From Figure 3, it can be seen that as the pump beam radius increases, the temperature at the center of the laser medium

starts to decrease. This is mainly because the relationship between the pump beam radius and the heat power density is inversely proportional, so the heat accumulated at the laser medium's end face decreases. The specific temperature distribution along the radial direction is shown in Figure 4, which illustrates the heat distribution at the laser medium's end face under different pump beam radii.

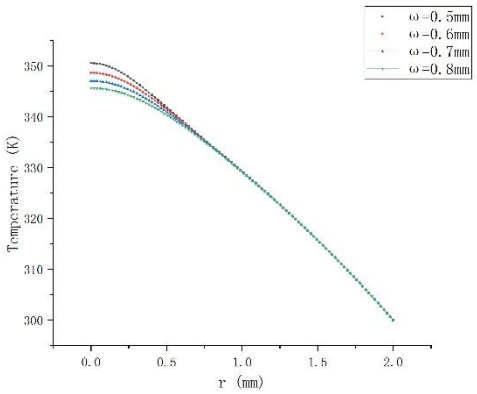

Figure 4 Radial Temperature Distribution of the Laser Medium under Different Pump Beam Radii

When the pump beam radius is 0.05 cm, 0.06 cm, 0.07 cm, and 0.08 cm, the center temperature of the laser medium end face is 350.52K, 348.63K, 347.03K, and 345.63K, respectively. After the pump beam radius decreases, the temperature at the end face decreases overall, but the decrease is very slow, with a temperature reduction controlled within 2K. Therefore, in practical applications, the choice of pump beam radius mainly depends on the requirements of the laser beam.

4 NUMERICAL SIMULATION OF THE LASER MEDIUM END-FACE TEMPERATURE

This section uses the fourth-order Runge-Kutta [9] method to numerically solve the heat conduction equation, simulate the temperature distribution at the laser medium's end face, and investigate the impact of pump power and pump beam radius on the end-face temperature distribution.

4.1 Influence of Pump Power on Medium Temperature Distribution

Figure 5 shows the three-dimensional temperature distribution at the laser medium's end face when the Nd:YAG rod has a radius and length of 0.2 cm and 0.5 cm, respectively, and the pump power is 5W, 10W, 15W, and 20W, with a pump beam radius of 0.5 mm.

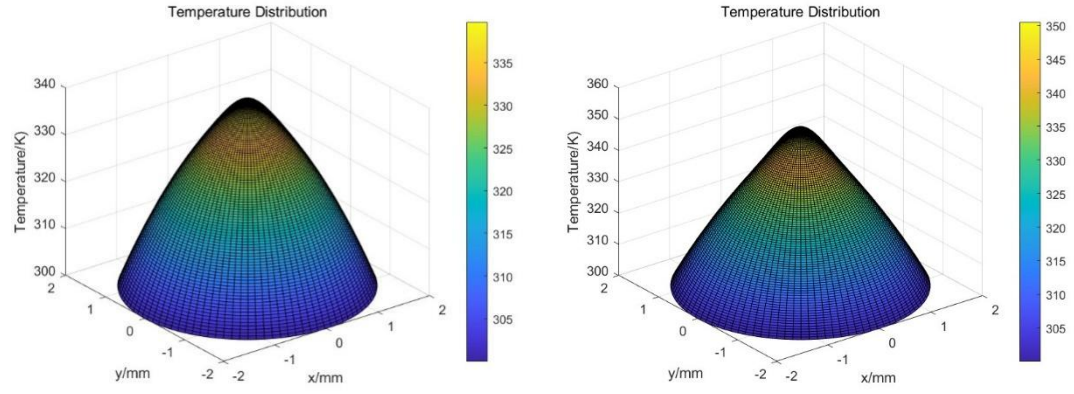

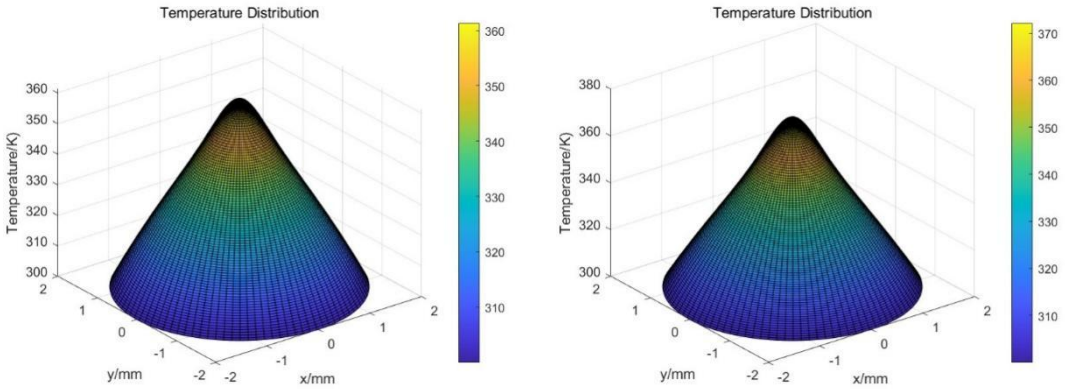

Figure 5: Temperature Distribution at the End-Face of the Laser Medium under Different Pump Powers

From Figure 5, it can be seen that along the radial direction, the temperature at the center is the highest, and it increases as the pump power increases. As the pump power increases, the energy absorbed by the laser medium also increases, leading to more heat accumulation at the smaller end face. The temperature distribution along the radial direction is shown in the figure 6.

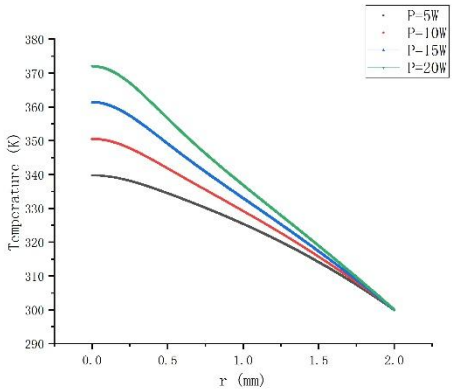

Figure 6 Radial Temperature Distribution of the Laser Medium under Different Pump Powers

Figure 6 shows the heat distribution at the laser medium's end face under different pump powers. The center temperature of the laser medium's end face is 339.74K, 350.53K, 361.32K, and 372.11K for pump powers of 5W, 10W, 15W, and 20W, respectively.

4.2 Influence of Pump Beam Radius on Medium Temperature Distribution

Figure 7 shows the three-dimensional temperature distribution at the laser medium's end face when the Nd:YAG rod has a radius and length of 0.2 cm and 0.5 cm, respectively. The pump power is fixed at 10W, and the pump beam radii are 0.05 cm, 0.06 cm, 0.07 cm, and 0.08 cm.

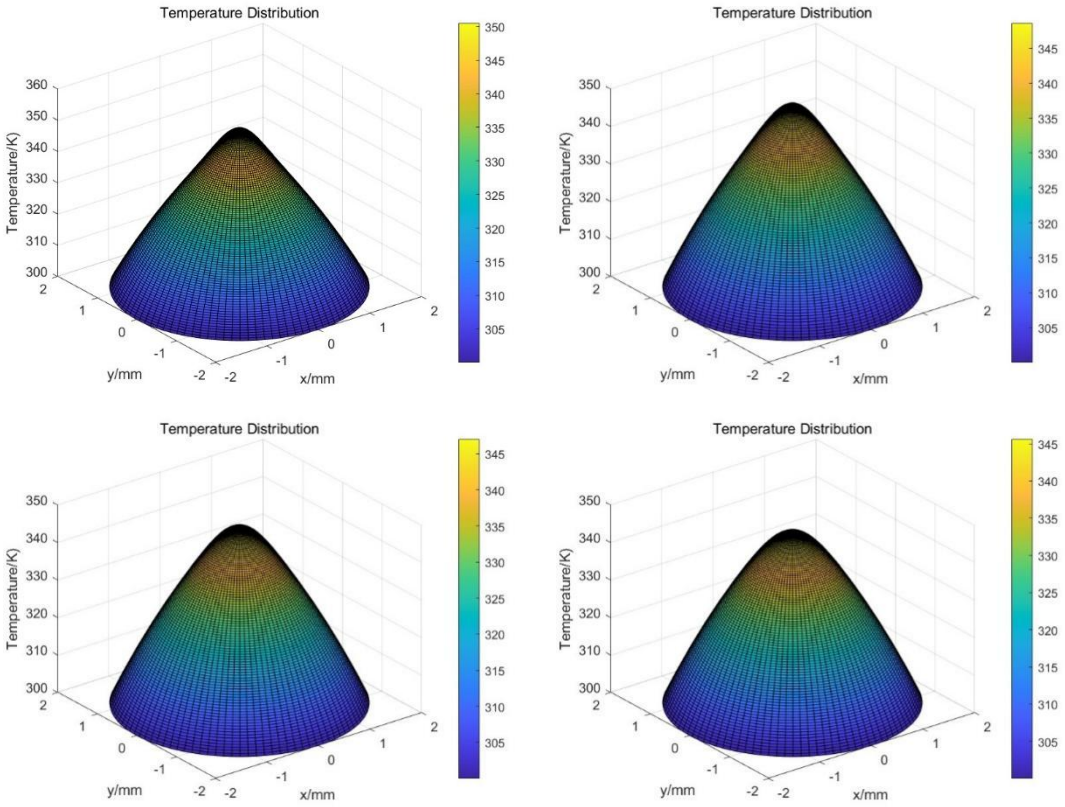

Figure 7 Temperature Distribution at the End-Face of the Laser Medium under Different Pump Beam Radii

From Figure 7, it can be seen that after the pump beam radius increases, the temperature at the center of the laser medium starts to decrease. This is mainly because the relationship between the pump beam radius and the heat power density is inversely proportional, so the heat accumulated at the laser medium's end face decreases. The specific temperature distribution along the radial direction is shown in Figure 8, which illustrates the heat distribution at the laser medium's end face under different pump beam radii.

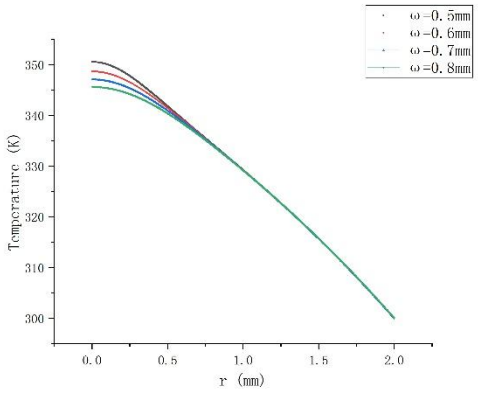

Figure 8 Radial Temperature Distribution of the Laser Medium under Different Pump Beam Radii

When the pump beam radius is 0.05 cm, 0.06 cm, 0.07 cm, and 0.08 cm, the center temperature of the laser medium's end face is 350.53K, 348.64K, 347.03K, and 345.64K, respectively.

5 COMPARISON BETWEEN NUMERICAL AND ANALYTICAL SIMULATIONS

The fourth-order Runge-Kutta method is used to convert the partial differential equation to an ordinary differential equation and then perform the calculation. A power series method is used to derive the analytical expression for the temperature distribution. This section compares the numerical results with the analytical calculations to verify the correctness of the analytical expression.

Table 1 Comparison of Analytical and Numerical Solutions for End-Face Center Temperature under Different Parameters

Parameters	Analytical calculation (K)	Numerical calculation (K)	Relative error (%)

Pump power (W)	5	339.7300	339.7373	0.0022
	10	350.5200	350.5290	0.0026
	15	361.3150	361.3207	0.0016
	20	372.1050	372.1124	0.0020
Pump beam radius (cm)	0.05	350.5200	350.5290	0.0026
	0.06	348.6300	348.6381	0.0023
	0.07	347.0250	347.0334	0.0024
	0.08	345.6300	345.6379	0.0023

From Table 1, it can be seen that, under different pump powers and pump beam radii, the analytical solution obtained by the analytical method is slightly smaller than the numerical solution obtained by the fourth-order Runge-Kutta method. The average error between the two methods for different pump powers is 0.0021%, and for different pump beam radii, the average error is 0.0024%. As the relevant parameters change, the error between the analytical solution and the numerical solution of the temperature distribution obtained by the two methods is small, with precision up to two decimal places. The simulation results derived from the analytical expression using the series method are very close to those obtained by the fourth-order Runge-Kutta method, and the two methods show excellent consistency, with relative errors controlled within 0.01%. This effectively verifies the correctness of the series method used in the calculations.

The analytical method uses series expansion for solving, and in the calculation process, truncation errors and approximations lead to certain errors. Although the analytical method itself is exact, numerical errors (such as floating-point errors) may affect the final results. Especially when there are many iterations or large numerical ranges involved, precision limits can cause computational errors. The main feature of numerical methods is that they discretize continuous problems, which brings some inherent errors. Since computers can only handle a finite number of digits, numerical methods also introduce unavoidable errors during the calculation. Particularly, when iterating multiple times or solving complex equations, rounding errors can accumulate, affecting the final result.

Both the analytical and numerical calculations of the temperature distribution in the laser medium of the solid-state laser give consistent trends, and this result fully confirms the rationality of using the series method in the derivation. In the calculation of the heat conduction equation for the laser medium in the solid-state laser, solving the heat model established in this paper using the power series method is a relatively simple and more easily understood approach. Ultimately, an analytical expression for the end-face temperature distribution is obtained, which helps in further studying the relationship between temperature distribution and variables, and is of significant physical importance in understanding the thermal effects in solid-state lasers.

COMPETING INTERESTS

The authors have no relevant financial or non-financial interests to disclose.

REFERENCES

[1] Chen S, Huang H, Chen H. Study on the effect of thermal effect dimensions on the output performance of solid-state lasers. Laser Journal 2016, 37(10): 14-17.

[2] Kim M Kwon G P, Lee J. Fully analytic approach to evaluate laser-induced thermal effects. Current Optics and Photonics 2017, 1(6): 649-654.

[3] Xiao Qirong, Zhang Dayong, Wang Zhehui, et al. A review of high-power fiber laser pumping coupling technologies. Chinese Journal of Lasers 2017, 44(02): 112-129.

[4] Chen Q, Wang M, Pan N, et al. Optimization principles for convective heat transfer. Energy 2009, 34(9): 1199-1206.

[5] AbdulRazzaq M J, Mohammed A Z, Abass A K, et al. A new approach to evaluate temperature distribution and stress fracture within solid state lasers. Optical and Quantum Electronics 2019, 51: 1-10.

[6] AbdulRazzaq M J, Shibib K S, Younis S I. Temperature distribution and stress analysis of end pumped lasers under Gaussian pump profile. Optical and Quantum Electronics 2020, 52(8): 379.

[7] Martin Maillard, Gabriel Amiard-Hudebine, Marc Tondusson, et al. Kinetics and wavelength dependence of thermal and excited-state population on lens effect induced in a Nd:YAG rod amplifier. Opt. Express 2023, 31: 1799-1812.

[8] Du Wen. Analytical study of the heat conduction equation of the laser medium in solid-state lasers. Doctoral dissertation, Xi'an Technological University, 2023.

[9] Huang Xiaohong, Hu Zhenhua. A brief analysis of the Runge-Kutta method. Heilongjiang Science and Technology Information 2012, 2012(23): 28.